Results in Physics 15 (2019) 102535

Contents lists available at ScienceDirect

Results in Physics

journal homepage: www.elsevier.com/locate/rinp

Evolution of Fe-containing intermetallic phases and abnormal grain growth in 6063 aluminum alloy during homogenization

Kanokwan Uttarasak[a], Wanchai Chongchitnan[b], Kenji Matsuda[c], Torranin Chairuangsri[d], Julathep Kajornchaiyakul[e], Chaiyasit Banjongprasert[f,g,*]

[a] Ph.D. Degree Program in Materials Science, Department of Physics and Materials Science, Faculty of Science, Chiang Mai University, Chiang Mai 50200, Thailand
[b] CAP C.E.L. CO., LTD, Klong Luang, Klong 6, Pathumthani 12120, Thailand
[c] Department of Materials Design and Engineering (MaDE), Faculty of Sustainable Design, Graduate School of Science and Engineering for Research, University of Toyama, Gofuku, Toyama 9308555, Japan
[d] Department of Industrial Chemistry, Faculty of Science, Chiang Mai University, Chiang Mai 50200, Thailand
[e] National Metal and Materials Technology Center (MTEC), Klong Luang, Pathumthani 12120, Thailand
[f] Department of Physics and Materials Science, Faculty of Science, Chiang Mai University, Chiang Mai 50200, Thailand
[g] Center of Excellence in Materials Science and Technology, Chiang Mai University, Chiang Mai 50200, Thailand

ARTICLE INFO

Keywords:
6063 aluminum alloy
Abnormal grain growth
Homogenization
Ex-situ characterization
Zener pinning

ABSTRACT

The 6063 aluminum billet alloy has been widely used as raw materials for aluminum extrusion profiles. A high-quality billet for good extrusion products is provided from a heat treatment process called homogenization. This process can give a homogeneous microstructure by reducing microsegregation and dissolving intermetallic phases. However, homogenization can create a very large grain size (abnormal grains) in 6063 aluminum billets. Fe content is one of the main factors that is strongly related to abnormal grain growth because Fe can form Fe-containing intermetallic phases in 6063 aluminum structure. The morphology and volume fraction of Fe-containing intermetallic phases are subjected to change during homogenization. These results relate to a decrease in the volume fraction of intermetallics, which corresponds to the Zener pinning pressure, grain boundary migration, and abnormal grain growth. Therefore, this study aims to understand the evolution of Fe-containing intermetallic phases on abnormal grain growth in 6063 aluminum billets during homogenization. Ex-situ characterization by energy dispersive spectrometer (EDS) and electron backscattered diffraction (EBSD) was performed on 6063 aluminum alloy to gain an in-depth understanding of abnormal grain growth.

Introduction

Abnormal grain growth in polycrystalline materials is defined when the grain size is in millimeters. The main factors that induce abnormal grain growth include (1) texture (2) second-phase particles and (3) surface effects [1]. Aluminum and its alloys can be susceptible to abnormal grain growth after high-temperature processing [2–4]. 6063 is one of the most widely used aluminum alloys in the wrought product form. The raw materials, 6063 aluminum alloy is normally cast into a billet by a vertical direct chill casting machine before secondary processing [5]. Sometimes, abnormal grain growth can happen in 6063 aluminum alloy after homogenization due to a decrease in intermetallic phases on microstructure. The typical microstructure of as-cast 6063 contains aluminum matrix and Fe-containing intermetallic phases of β-Al_5FeSi located at the grain boundaries and Mg_2Si [6] due to the low solubility limit of Fe, Si, and Mg in the aluminum matrix [7]. The β-Al_5FeSi phase can be detrimental for extruded products. Therefore, the homogenization, a heat treatment process, is normally used to improve billet quality by breaking down and transforming the needle shape β-Al_5FeSi to a more spheroidal α-Al_8Fe_2Si. Whereas, the Mg_2Si particles dissolved in an aluminum matrix during homogenization [8–10]. A sublattice model and compositional limit of selected AlFeSi intermetallic phases were reported by COST 507 [11] to identify a typical AlFeSi intermetallic particle. This method used the EDS technique on the AlFeSi phase to estimate Fe:Si atomic ratios for typical phase prediction. The Fe:Si ratio in the range of 1.28–3.83 is used to predict α-Al_2Fe_8Si particle [12] while the minimum Fe:Si atomic ratio of 1.00 or 1.00 ± 0.25 can be used to predict β-Al_5FeSi particle [12,13]. In addition, for a better prediction of β to α transformation during homogenization of Mn-containing 6xxx alloys, the Fe(+Mn): Si should be used for calculation [14,15]. The influence of Mn on the Fe-containing intermetallic phases was also reported by Gao et al. [16].

* Corresponding author at: Department of Physics and Materials Science, Faculty of Science, Chiang Mai University, Chiang Mai 50200, Thailand.
E-mail address: chaiyasit.b@cmu.ac.th (C. Banjongprasert).

https://doi.org/10.1016/j.rinp.2019.102535
Received 11 May 2019; Received in revised form 18 July 2019; Accepted 23 July 2019
Available online 26 July 2019

Table 1
The chemical composition of 6063 aluminum billets in this study.

Sample	wt.%					
	Si	Fe	Mn	Mg	Ti	Al
I	0.397	0.089	0.002	0.530	0.0117	Balance.
II	0.419	0.170	0.034	0.517	0.0130	Balance.
III	0.429	0.081	0.001	0.517	0.0130	Balance.

For aluminum and its alloys, abnormal grain growth can occur in both non-deformed and deformed alloys after heat treatments. The tendency of abnormal grain growth in these alloys is generally determined by the inhibition of boundary migration by particles during annealing-related processes, as reported by Xu et al. [17]. The α-AlFe(Mn,Cr)Si dispersoid in a compressed Al-Mg-Si-Cu provided strong inhibition of boundary movements and prevented abnormal grain growth at elevated temperature [17]. Besides, the retardation of abnormal grain growth during hot deformation in friction stir welded 5083 aluminum alloy after heat treatment can be improved by increasing the volume fraction of intermetallic phases [18].

Moreover, it was found that β-Al_5FeSi had a strong influence on the grain size of 6063 aluminum alloy. It could prevent excessive grain growth after thermal heat treatment [19]. The literature confirms that second-phase particles have a strong influence on abnormal grain growth in metal. The effect of second phase particles in metallic materials on abnormal grain growth can be discussed in terms of Zener pinning pressure [20,21]. If the alloy contains a high volume fraction of second phases, it will give a high pinning pressure and prevents abnormal grain growth. From the model proposed by Humphreys [20] relating to particle pinning parameter (Ψ), abnormal grain growth will occur when the particle pinning parameter in metal is between 0.25 and 1.0. However, if the particle pining parameter in metal is higher than 1.0, they propose that there is no grain growth in metal [20]. It is well known that the homogenization process leads to the dissolving and transforming of needle shape of β-Al_5FeSi to the spheroidal phase of α-Al_8Fe_2Si. Hence, the volume fraction of the second phases will be changed during homogenization. However, there is no direct observation of the microstructural evolution of as-cast 6063 aluminum alloy, especially with the different Fe contents, during homogenization. This study aims to understand the evolution of second phases that affects to abnormal grain growth in 6063 aluminum alloy during homogenization. In addition, the ex-situ experimental results were directly compared with the Humphreys' model to observe the validation of the model on the abnormal grain growth of 6063 aluminum alloy.

Materials and method

The 127 mm (5 in.) diameter of 6063 commercial aluminum billets cast by an AirSlip vertical direct chill casting were used in this study. Their compositions are listed in Table 1.

To monitor the evolution of intermetallic phases on abnormal grain growth during homogenization, the as-cast sample I and II (127 mm diameter, 5800 mm long) were cut into 8x10x4 mm^3, as shown in Fig. 1. Square samples I and II were selected 10 mm from the billet outer diameter to avoid any inhomogeneous microstructure and composition in each sample. The samples I and II were homogenized in a heat-resistant furnace at 585 °C for various times from 1 to 720 min.

The top side of each sample was used for microstructure investigation, and the bottom side was used for macrostructure analysis. For microstructure analysis, an area in each sample was marked by Vickers's indentation for SEM/EDS and SEM/EBSD observation. Results are from a fixed (same) area and so-called 'ex-situ' characterization. For EDS and EBSD analysis, the sample was prepared using a conventional metallographic technique following by 4 h of vibration polishing with a colloidal silica suspension. SEM/EDS and SEM/EBSD were run under a JEOL scanning electron microscope JSM-IT 300 LV operating at 15 kV and 20 kV consequently. EBSD maps were acquired with step sizes of 1 μm. The HKL channel 5 software of Oxford instrument was used to analyze EBSD data. TEM under a JEOL transmission electron microscope JEM-4010 T at 400 kV was used for characterization of intermetallic phases. The thin sample for TEM was prepared by focus ion beam (FIB) on the Hitachi Dual Beam FB-2100.

Results and discussion

Evolution of intermetallics during homogenization at 585 °C

According to a backscatter electron image (BSI) of an as-cast microstructure in samples I and II, shown in Figs. 2 and 3, it was found that the microstructure in both samples I and II changed during homogenization at 585 °C. The SEM/EDS results indicated that bright particles in both as-cast structures in samples I and II were β-Al_5FeSi intermetallic particles while dark particles were Mg_2Si. The results show similar microstructure as seen in a typical microstructure of as-cast 6063 billets [5,22]. These results were confirmed by the analytical chemical composition of AlFeSi intermetallic particles as shown in Tables 2 and 3. The Fe:Si atomic ratio of intermetallic particles from EDS in as-cast samples I and II were close to 1.00, indicating β-Al_5FeSi intermetallic particles [12]. In addition, after using TEM/EDS was used to characterize the remaining intermetallic phases on abnormal grain growth of 6063 sample (sample III) (Fig. 4) homogenized at 585 °C in industrial furnace for 150 min. The chemical composition of

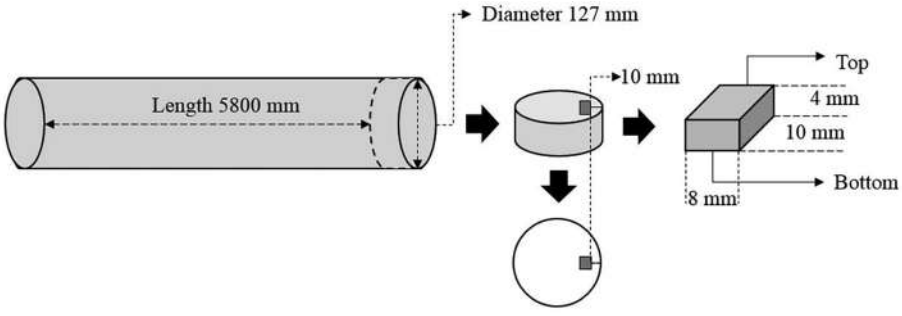

Fig. 1. Schematic diagram of 6063 aluminum alloy for microstructure and macrostructure analysis.

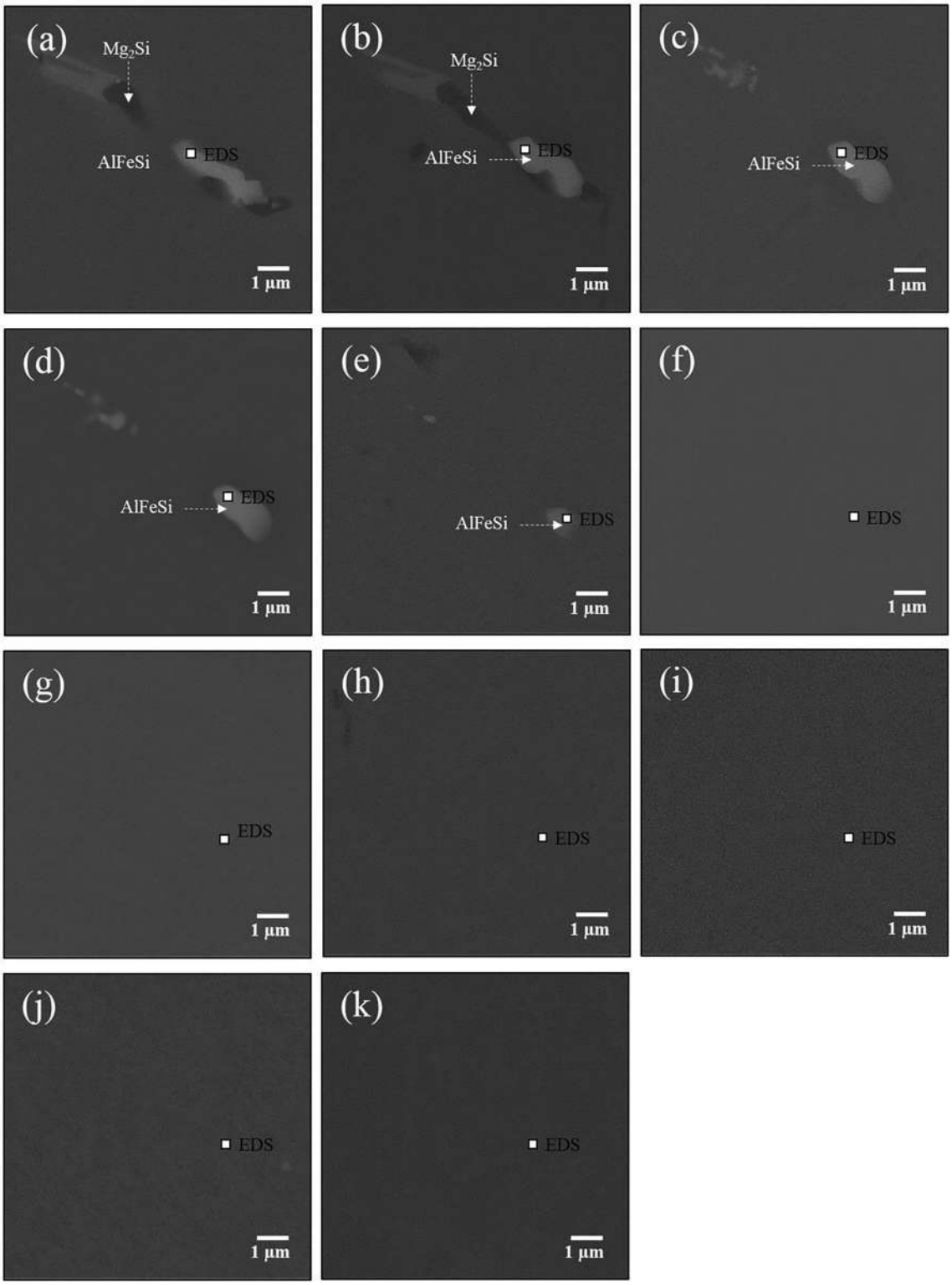

Fig. 2. BSI images from 6063 aluminum sample I (a) as-cast sample and (b–k) homogenized at 585 °C for (b) 1 min, (c) 5 min, (d) 10 min, (e) 30 min (f) 60 min, (g) 120 min, (h) 150 min, (i) 300 min, (j) 600 min and (k) 720 min.

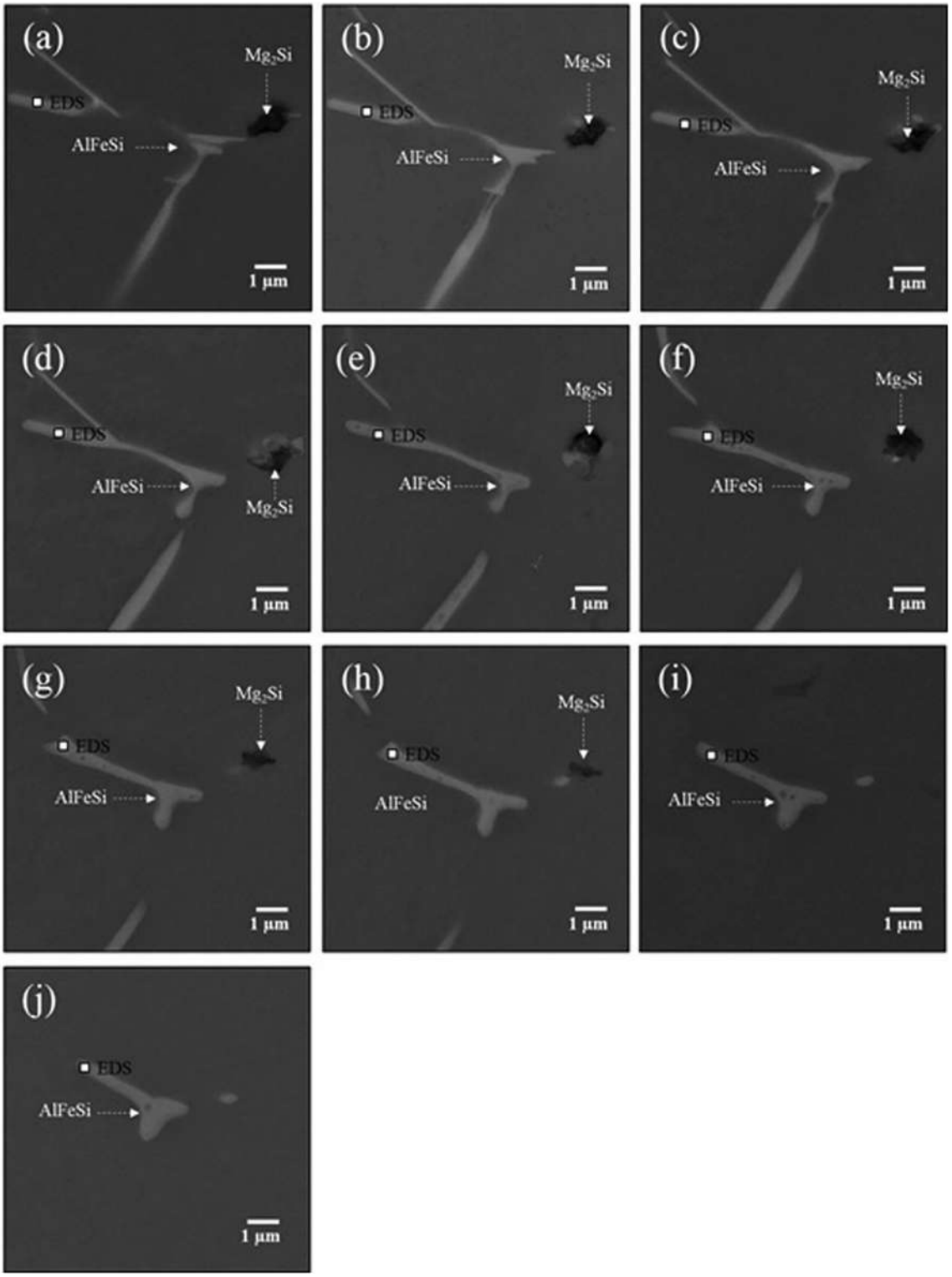

Fig. 3. BSI images from 6063 aluminum sample II (a) as-cast sample and (b–j) homogenized at 585 °C for (b) 1 min, (c) 5 min, (d) 10 min, (e) 30 min, (f) 60 min, (g) 120 min, (h) 150 min, (i) 300 min, (j) 600 min.

Table 2
Chemical composition of the intermetallic phases of 6063 aluminum sample I using SEM/EDS characterization.

Homogenizing holding time	Elementary (atomic%)					Ratio	Prediction Phases
	Mn	Mg	Al	Fe	Si	Fe:Si	
As-cast	–	1.41	83.53	7.74	7.33	1.06	β-Al_5FeSi
1 min	–	5.40	75.08	8.73	10.79	0.81	β-Al_5FeSi
5 min	–	–	84.84	8.80	6.37	1.38	α-Al_8Fe_2Si
10 min	–	–	85.90	8.26	5.83	1.42	α-Al_8Fe_2Si
30 min	–	–	94.16	3.22	2.62	1.23	β-Al_5FeSi
60 min	–	–	99.17	–	0.83	–	Al matrix
120 min	–	–	98.81	–	1.19	–	Al matrix
150 min	–	–	99.14	–	0.86	–	Al matrix
300 min	–	–	99.31	–	0.61	–	Al matrix
600 min	–	–	98.79	–	1.21	–	Al matrix
720 min	–	–	99.36	–	0.64	–	Al matrix

Table 3
Chemical composition of the intermetallic phases of 6063 aluminum sample II using SEM/EDS characterization.

Homogenizing holding time	Elementary (atomic%)					Ratio	Prediction Phases
	Mn	Mg	Al	Fe	Si	Fe:Si	
As-cast	–	–	88.63	4.91	6.46	0.76	β-Al_5FeSi
1 min	–	–	88.36	4.95	6.69	0.74	–
5 min	–	–	87.22	5.47	7.31	0.75	β-Al_5FeSi
10 min	–	–	88.86	4.64	6.50	0.71	–
30 min	–	–	90.24	5.38	4.38	1.23	β-Al_5FeSi
60 min	–	–	89.92	6.62	4.29	1.54	α-Al_8Fe_2Si
120 min	0.44	–	88.33	6.59	4.04	1.74	α-Al_8Fe_2Si
150 min	–	–	90.16	5.83	4.01	1.45	α-Al_8Fe_2Si
300 min	0.67	–	90.36	4.98	3.99	1.42	α-Al_8Fe_2Si
600 min	0.84	–	90.40	4.99	3.77	1.55	α-Al_8Fe_2Si

intermetallic phases is shown in Table 4. The average chemical composition of intermetallic particle in weight% as illustrated in Table 4 were Al = 60.99, Si = 12.38, and Fe = 26.63. These values were in the same range as Al, Si, and Fe element values of β-Al_5FeSi intermetallic particles that were recorded in JCPDS card no. 00-049-1499 database [23]. These results confirmed that the intermetallic particle was β-Al_5FeSi. Furthermore, the average Fe:Si EDS in both weight ratio [8] and in atomic ratio [12] of intermetallic particles from Table 4 were 2.0 and 1.0 confirming β-Al_5FeSi. During homogenization, Mg_2Si particles were dissolved through an aluminum matrix. The absence of dark Mg_2Si was observed when homogenizing holding time increased as seen in Fig. 2(a–c) and (Fig. 3(a–i)). Considering the marked area of sample I, it was found that the β-Al_5FeSi gradually transformed from a needle shape into a more spheroidal shape by dissolving β-Al_5FeSi particles [24,25] through the aluminum matrix when the homogenizing holding time increased as shown in Fig. 2(a–k). For the marked area in sample II (Fig. 3(a–j)), the β-Al_5FeSi was broken up from a β-Al_5FeSi network. These changes remained after homogenization at 585 °C for 600 min holding time when compared to β-Al_5FeSi in the marked area in sample I. This particle disappeared after homogenization at 585 °C for 60 min. The remaining intermetallic particle in sample II was α-Al_8Fe_2Si intermetallic phase. These results are similar to the prediction proposed by Hosseinifar and Malakhov [12].

It was found that the dissolving Mg_2Si particles and phase transformation of intermetallic particles in the sample I was faster than that of sample II. The Mg_2Si in the sample I was dissolved within 5 min after homogenization at 585 °C while sample II was 300 min. In the same way, the phase transformation time from β-Al_5FeSi into α-Al_8Fe_2Si in the sample I was faster than that in sample II. These results correlated to the initial grain size of the as-cast structure before homogenization. The average grain size of as-cast structure of sample I was 74 μm and smaller than that of sample II (93 μm) as shown in Fig. 5(a) and (c). Hence, the dissolving and transformation of intermetallic particles in the sample I were faster than in sample II due to the short diffusion distance at a high homogenization temperature [26]. In addition, the intermetallic particles of β-Al_5FeSi and α-Al_8Fe_2Si were located at the grain boundaries of the 6xxx alloys, whereas Mg_2Si particles precipitated in both aluminum matrixes and on the surface of β-Al_5FeSi [24,25]. Therefore, the β to α phase transformation and particle dissolution can result in a less retarding grain boundary migration due to a decrease in intermetallic particles at grain boundaries. The volume fraction of intermetallic particles in both samples I and II decreased

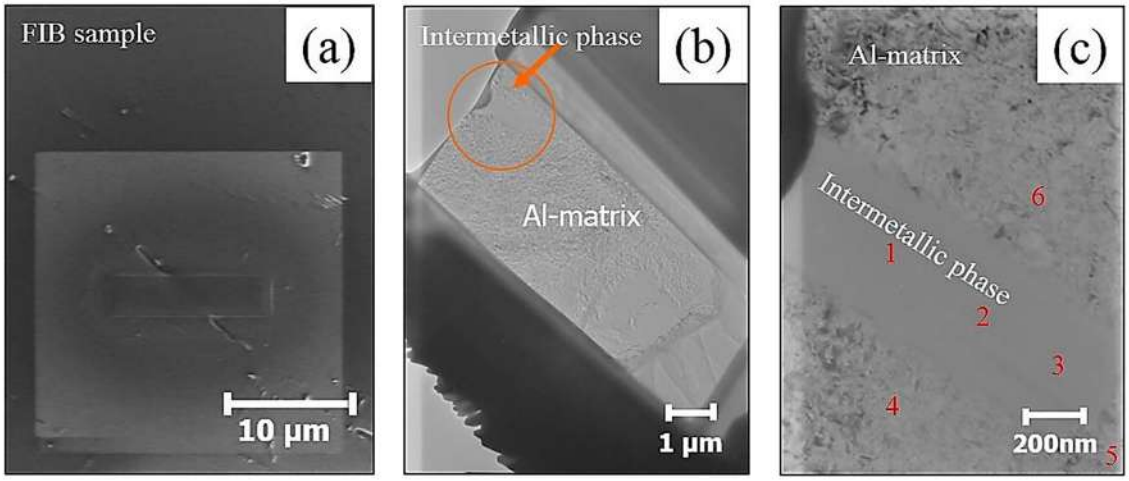

Fig. 4. TEM micrographs for 6063 aluminum alloy sample III; abnormal grain growth of (a) the intermetallic phase sample using FIB preparation (b) a bright field image of the intermetallic phase and the aluminum matrix at low magnification (c) a bright field image of the intermetallic phase and the aluminum matrix at high magnification.

Table 4
Chemical composition of the intermetallic phases in 6063 aluminum sample III using TEM/EDS characterization.

Point	Location	Weight%				Atomic%			
		Al	Si	Fe	Fe:Si	Al	Si	Fe	Fe:Si
1	Intermetallic phase	60.99	12.47	26.54	2	71.09	13.97	14.96	1.07
2	Intermetallic phase	60.74	12.28	26.97	2	70.98	13.79	15.23	1.10
3	Intermetallic phase	61.25	12.39	26.37	2	71.31	13.86	14.83	1.07
4	Aluminum matrix	96.16	O = 3.84			96.16	O = 6.30		
5	Aluminum matrix	96.64	O = 3.36			94.46	O = 5.54		
6	Aluminum matrix	95.72	O = 4.28			92.99	O = 7.01		
Possible intermetallic phase		β-Al_5FeSi				β-Al_5FeSi			

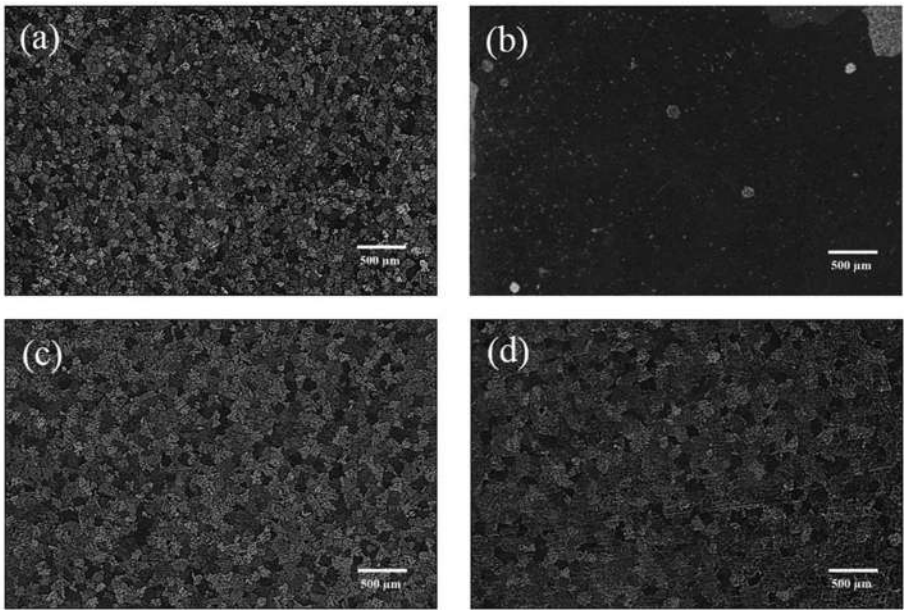

Fig. 5. Optical micrographs from aluminum sample I (0.089wt.%Fe) at (a) as-cast, (b) homogenized at 585 °C for 600 min holding time and sample II (0.170wt.%Fe) at (c) as-cast, (d) homogenized at 585 °C for 600 min.

Table 5
Average volume fraction, average particle diameters, average grain size, and particle pinning parameter for various homogenizing holding time of 6063 aluminum alloys sample I.

Homogenizing holding time	Volume fraction	Particle size (μm)	Average grain size (μm)	Particle pinning parameter (Ψ)
As-cast	0.004970 ± 0.00080	0.813 ± 0.32	74 ± 7	1.35 ± 0.14
1 min	0.005660 ± 0.00080	0.908 ± 0.36	85 ± 3	1.60 ± 0.19
5 min	0.005438 ± 0.00090	0.883 ± 0.46	91 ± 1	1.68 ± 0.24
10 min	0.005004 ± 0.00050	0.865 ± 0.45	105 ± 3	1.81 ± 0.24
30 min	0.004310 ± 0.00010	0.971 ± 0.33	104 ± 5	1.39 ± 0.15
60 min	0.002658 ± 0.00020	0.938 ± 0.32	104 ± 5	0.89 ± 0.09
120 min	0.002876 ± 0.00080	0.980 ± 0.35	100 ± 5	0.88 ± 0.14
150 min	0.002188 ± 0.00030	0.923 ± 0.37	107 ± 3	0.76 ± 0.10
300 min	0.002022 ± 0.00004	1.081 ± 0.23	110 ± 9	0.61 ± 0.05
600 min	0.002027 ± 0.00006	0.925 ± 0.14	124 ± 8	0.82 ± 0.04
720 min	0.001782 ± 0.00007	1.168 ± 0.28	103 ± 14	0.33 ± 0.06

Table 6
Average volume fraction, average particle diameters, average grain size, and particle pinning parameter for various homogenizing holding time of 6063 aluminum alloys sample II.

Homogenizing holding time	Volume fraction	Particle size (μm)	Average grain size (μm)	Particle pinning parameter (Ψ)
As-cast	0.011326 ± 0.0013	0.717 ± 0.25	93 ± 2	4.41 ± 0.32
1 min	0.010020 ± 0.0009	0.567 ± 0.27	100 ± 3	5.29 ± 0.31
5 min	0.008848 ± 0.0003	0.696 ± 0.28	97 ± 2	3.69 ± 0.24
10 min	0.009164 ± 0.0009	0.677 ± 0.24	98 ± 1	4.00 ± 0.25
30 min	0.008700 ± 0.0004	0.665 ± 0.22	93 ± 2	3.65 ± 0.18
60 min	0.007854 ± 0.0008	0.671 ± 0.24	108 ± 4	3.79 ± 0.24
120 min	0.007352 ± 0.0005	0.824 ± 0.31	101 ± 3	2.71 ± 0.24
150 min	0.007308 ± 0.0007	0.717 ± 0.38	101 ± 3	3.10 ± 0.30
300 min	0.006818 ± 0.0005	0.736 ± 0.31	104 ± 4	2.90 ± 0.23
600 min	0.005848 ± 0.0004	0.861 ± 0.24	103 ± 4	2.10 ± 0.15

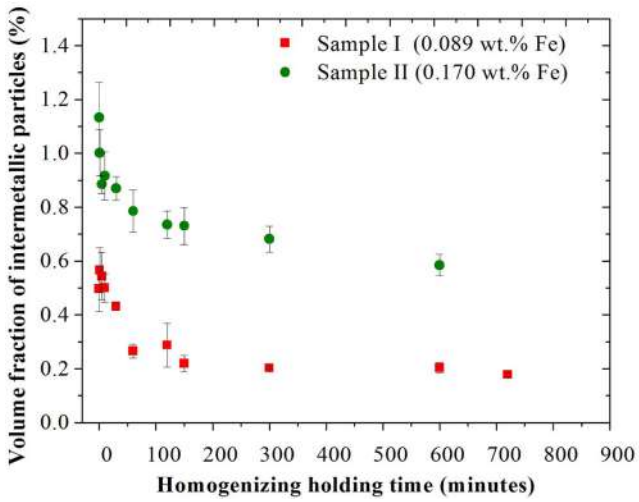

Fig. 6. The volume fraction of intermetallic particles in 6063 aluminum sample I and Sample II during homogenization at 585 °C.

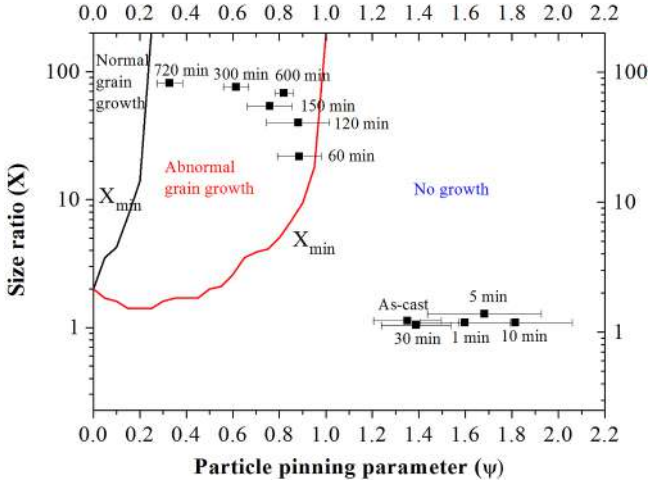

Fig. 7. Grain size ratio plot from sample I showing regions corresponding to grain growth mechanism predicted by Humphreys' Model [20].

with homogenizing holding time. The sample I had a low Fe content (0.089wt.%Fe) leading to a lower volume fraction of intermetallics when compared to sample II (0.170wt.%Fe). Hence, the sample I had a lower volume fraction of Fe-containing intermetallics after homogenization at 585 °C than sample II and resulted in a low retardation of grain boundary migration and hence abnormal grain growth during homogenization at 585 °C as shown in Fig. 5(b). The effect of volume fraction of Fe-containing intermetallics on abnormal grain growth behavior will be further discussed in Section "The volume fraction of intermetallic particles in 6063 aluminum alloy during homogenization".

The volume fraction of intermetallic particles in 6063 aluminum alloy during homogenization

The phase transformation of β-Al_5FeSi to α-Al_8Fe_2Si occurred when β-Al_5FeSi gradually dissolved in the aluminum matrix during homogenization [24,25] leading to a decrease in the volume fraction of intermetallic particles in both samples I and II during homogenization at 585 °C as shown in Tables 5, 6 and Fig. 6. These particles directly affected the retarding of grain boundary migration proposed by Zener drag [20,21]. The pressure that retarded grain boundary migration was commonly known as Zener pinning pressure as explained in Eq. (1) [20,21].

$$P_z = \frac{3F_v\gamma}{2r} \quad (1)$$

where P_z is Zener pinning pressure (J m^{-3}), F_v is volume fraction of intermetallic particles, γ is grain boundary energy (J m^{-2}), and r is radius of intermetallic particles (μm). According to Eq. (1), the higher volume fraction of intermetallics leads to a higher Zener pinning pressure and retardation of boundary movement and thus prevents abnormal grain growth. For example, it is estimated that after homogenized for 60 min, the Zener pinning pressure in sample II was ~4 times higher than that in sample I. In addition, the volume fraction of intermetallic particles in samples I and II was used to calculate the

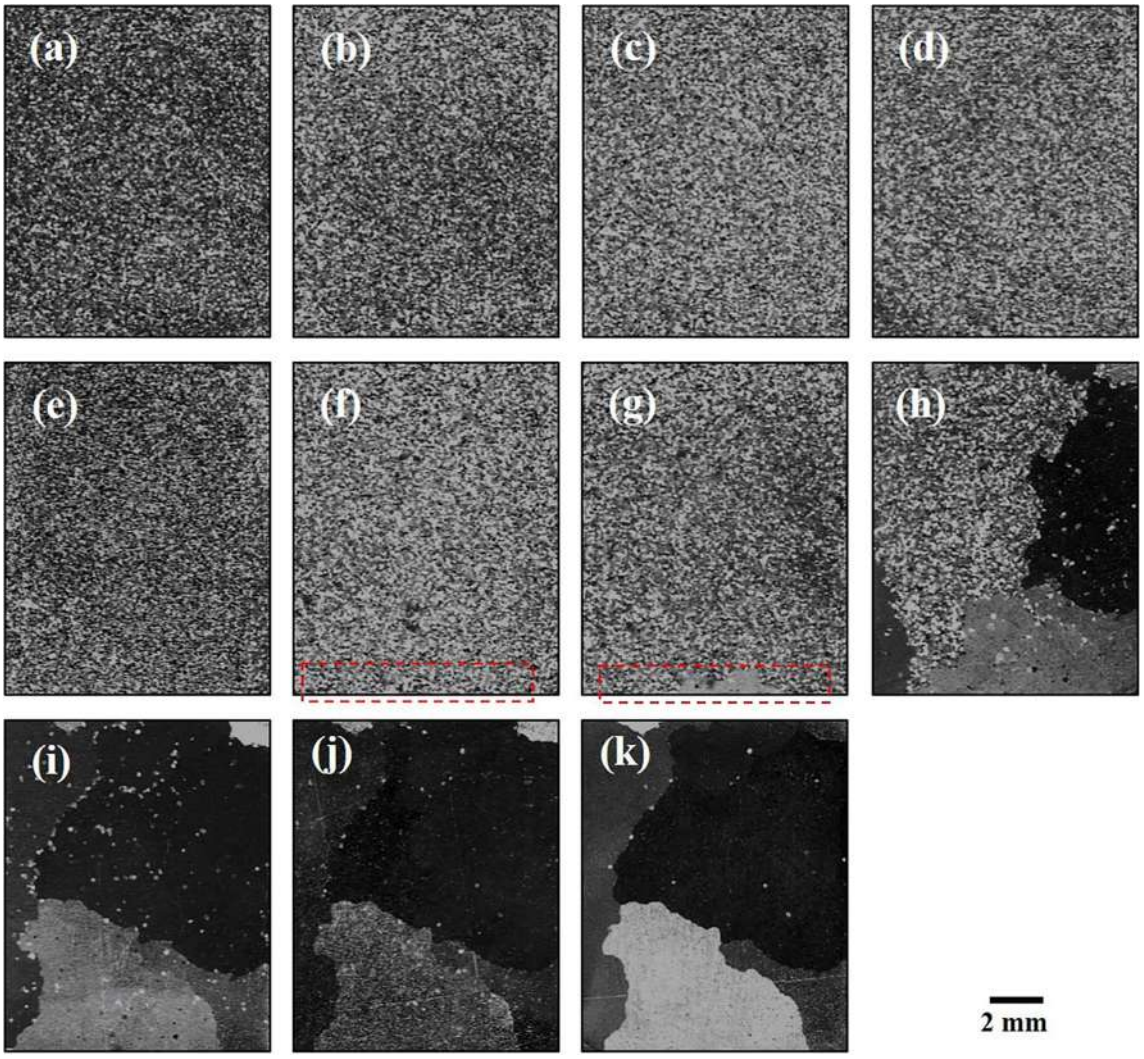

Fig. 8. Macrostructure from 6063 aluminum alloy sample I (a) as-cast sample and (b–k) are homogenized sample at 585 °C for (b) 1 min, (c) 5 min, (d) 10 min, (e) 30 min, (f) 60 min, (g) 120 min, (h) 150 min, (i) 300 min and (j) 600 min, and (k) 720 min.

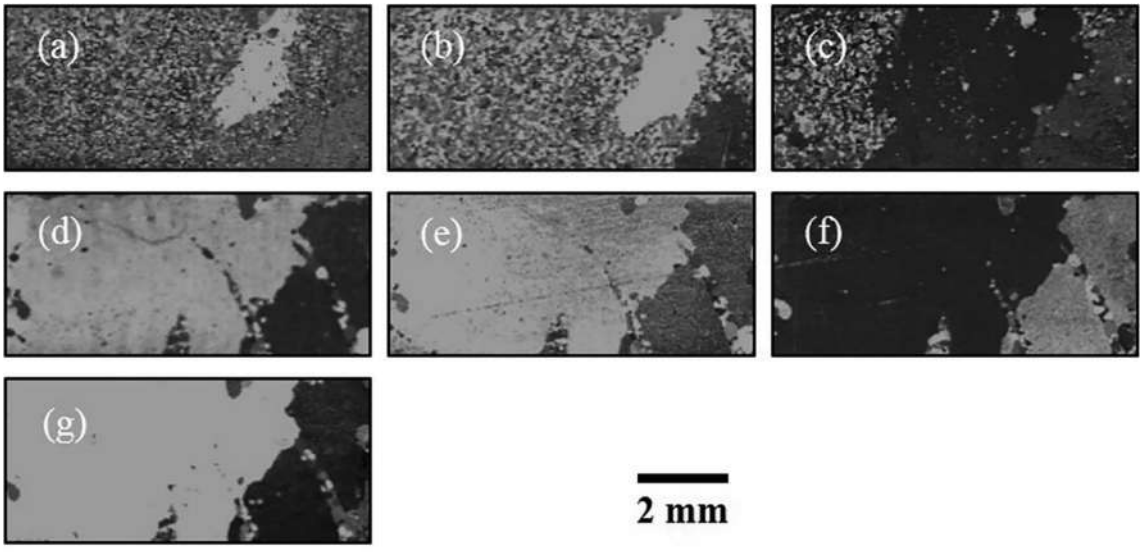

Fig. 9. Macrostructure from 6063 aluminum alloy sample I during homogenization at 585 °C for (a) 60 min, (b) 90 min, (c) 120 min, (d) 150 min, (e) 300 min, (f) 600 min, and (g) 720 min.

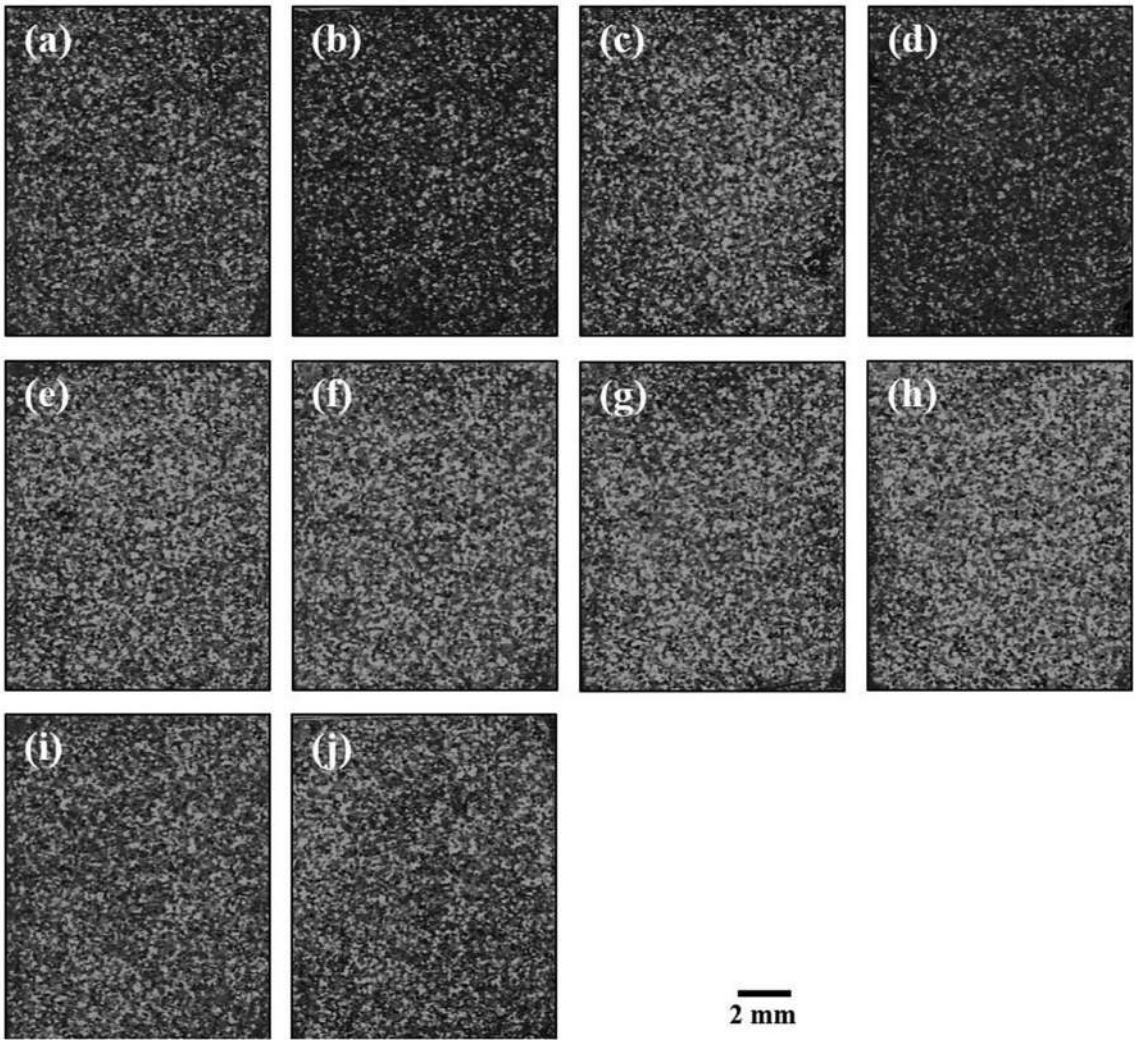

Fig. 10. Macrostructure from 6063 aluminum alloy sample II (a) as-cast sample and (b–j) are homogenized sample at 585 °C for (b) 1 min, (c) 5 min, (d) 10 min, (e) 30 min, (f) 60 min, (g) 120 min, (h) 150 min, (i) 300 min, and (j) 600 min.

particle pinning parameter (Ψ) to predict the tendency of abnormal grain growth during homogenization as seen in Humphreys' model [20] in Eq. (2).

$$\Psi = \frac{3F_v\bar{R}}{d} \tag{2}$$

where Ψ is particle pinning parameter, $\bar{R}$ is an average (mean equivalent) grain size (μm), and d is an average diameter of intermetallic particles (μm). This model can predict a tendency for abnormal grain growth during the heat treatment process. This growth can occur when a particle pinning parameter (Ψ) is within a range of 0.25–1.00. In addition, this model can be used to predict and explain the mechanism of abnormal grain growth in friction stir processing of aluminum alloy [27–30]. They stated that abnormal grain growth was related to particle pinning parameters. The particle pinning parameter of sample I and II during homogenization at 585 °C was shown in Tables 5 and 6.

Table 5 shows that particle pinning parameters of as-cast and the homogenized sample I at 585 °C for 1 min, 5 min, 10 min, 30 min were higher than 1.0. The Humphreys' model [20] (as shown in Fig. 7) can be applied to predict that there was no abnormal grain growth in 6063 aluminum structure after homogenization at 585 °C for 1 min, 5 min, 10 min, and 30 min. The particle pinning parameters in the sample I are 1.60, 1.68, 1.81, and 1.39 and within a range of 0.25–1.00 after homogenization at 585 °C for 60 min. This result predicted that the onset of abnormal grain growth of sample I was after homogenization at 585 °C for 60 min. This result was confirmed by the macrostructure as shown in Fig. 8, that shows the occurrence of abnormal grain growth in the macrostructure of sample I after homogenization at 585 °C for 60 min. The abnormal grain growth was clearly observed in a cross-section macrostructure as shown in Fig. 9(a). In addition, the small

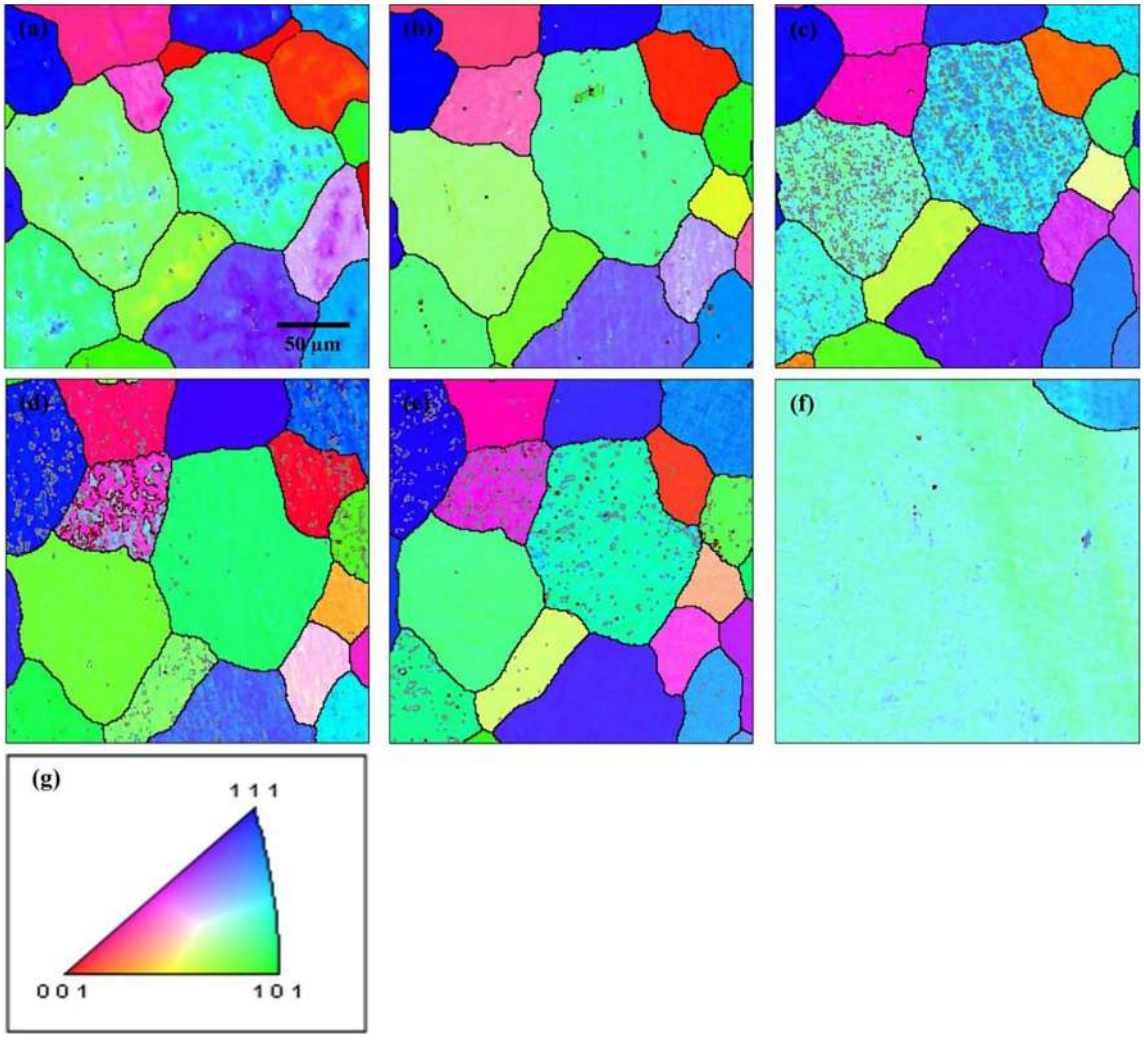

Fig. 11. EBSD maps for 1 sample from 6063 aluminum alloy sample I showing the aluminum phase (a) as-cast (b–f) are homogenized at 585 °C for (b) 30 min (c) 45 min (d) 60 min (e) 90 min (f) 120 min. (g) Orientation color key for maps. Grain boundaries are colored in accordance with misorientation angle range:$5^\circ < \theta < 10^\circ$ = gray, $10^\circ < \theta < 15^\circ$ = brown, and $\theta > 15^\circ$ = black. (For interpretation of the references to colour in this figure legend, the reader is referred to the web version of this article.)

grains that remained inside the abnormal grains were gradually disappeared with homogenizing holding time. This behavior was grain coalescence and later abnormal grain growth. However, there was no abnormal grain growth in sample II because the particle pinning parameter in Table 6 is not in a range of 0.25–1.00. These results were confirmed by the macrostructure of sample II, as shown in Fig. 10. The normal grain did not grow to abnormal grain growth when homogenizing holding times were increased. Therefore, the particle pinning model proposed by Humphreys [20] can be applied to predict the tendency of abnormal grain growth in 6063 aluminum alloy during homogenization.

Ex-situ EBSD investigation on abnormal grain growth in 6063 aluminum alloy during homogenization at 585 °C

To understand grain boundary migration and abnormal grain growth behavior, ex-situ EBSD was used to investigate the same area of the marked surface sample from low Fe (0.089wt.%Fe) content in as-cast 6063 aluminum sample I. Sample I was homogenized in a heat resistant furnace at 585 °C for various homogenizing holding times. For the ex-situ result, there was abnormal grain growth around the marked area after homogenization at 585 °C for 120 min as shown in Fig. 11(f). The change in the microstructure (as shown in Fig. 11) was related to a high migration rate of high angle grain boundaries [31]. These can be observed by the absence of high angle boundaries during

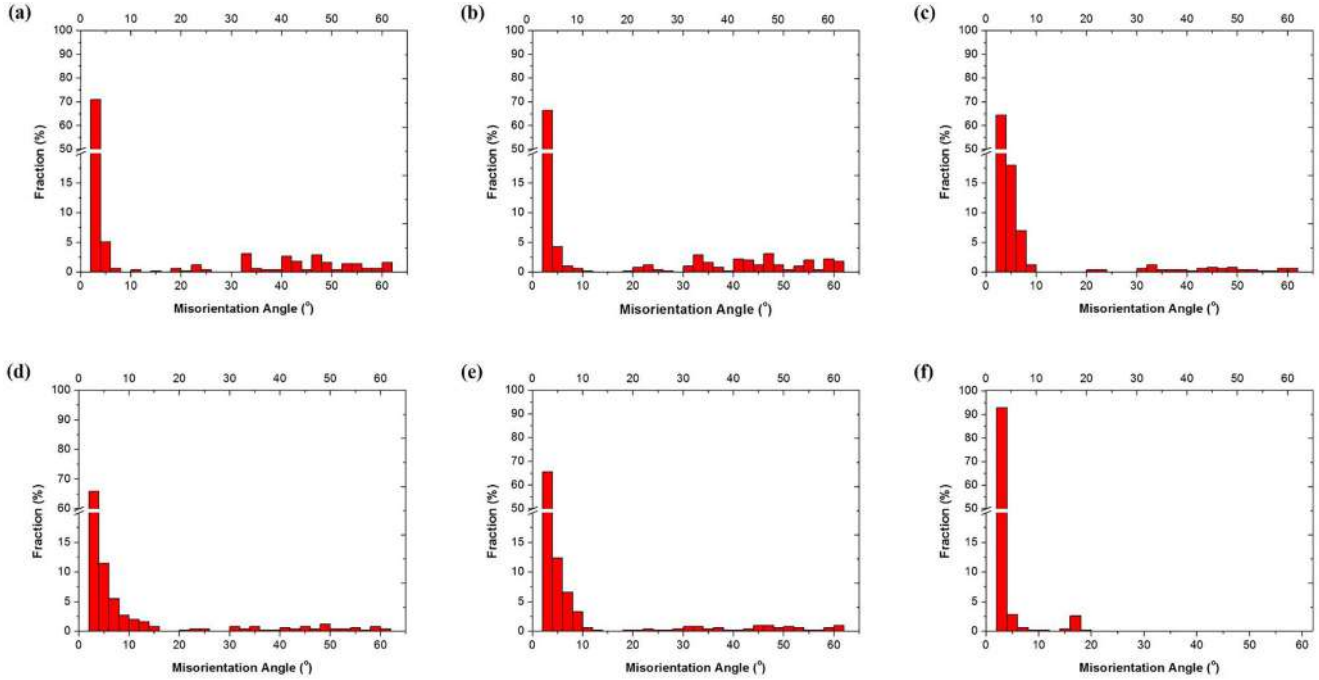

Fig. 12. Misorientation angle distribution for 1 sample from 6063 aluminum alloy sample I (a) as-cast and (b–f) are homogenized at 585 °C for (b) 30 min (c) 45 min (d) 60 min (e) 90 min (f) 120 min.

homogenization in Fig. 11(a–f); the black lines indicating high angle grain boundaries were mostly disappeared after homogenization at 585 °C for 120 min. Therefore, a high (grain) boundary movement in 6063 aluminum alloy billets during homogenization led to discontinuous recrystallization [32–35]. Fig. 12(a–f) shows a strong evidence of a reduction of the high misorientation angles during homogenization.

Moreover, the localized intermetallic particles in the 6063 aluminum structure was decreased when abnormal grain growth occurred during homogenization as shown in Fig. 13. Fig. 13 also shows the grain structure and the existence of Al, Fe, Si, Mg elements in 6063 structure during homogenization at 585 °C for 30 min, 45 min, 60 min, 90 min, and 120 min. The existence of Al, Fe, Si, and Mg elements in as-cast structure indicated the β-Al_5FeSi and Mg_2Si particles as previously mentioned. These elements were dissolved into an aluminum matrix after the homogenization as shown in Fig. 13. It was observed that the localized concentration of each element decreased with homogenizing holding times as shown in Fig. 13(a–f), and especially a decrease of Mg. This explained how Mg_2Si particles were dissolved into the aluminum matrix during homogenization at 585 °C. Therefore, the grain boundary migration and abnormal grain growth in 6063 aluminum alloy during homogenization correlated to discontinuous recrystallization, the phase transformation, and dissolving of the intermetallic particles during homogenization. The evidence of the distribution of intermetallic particles β-Al_5FeSi at the grain boundaries of sample II after homogenization at 585 °C for 600 min can be seen in BSI and corresponding EDS (red points) in the Fig. 14 and Table 7.

The evidence of the retardation of boundary movement can be seen in Fig. 15. In as-cast structure of sample II, grain 1 was surrounded by Fe-containing intermetallics at grain boundaries. However, after homogenization at 585 °C for 10 min, those Fe-containing intermetallics at grain boundaries dissolved and the grain 1 disappeared. Whereas, grain 2, with remaining Fe-containing intermetallics (as seen in Fig. 15(d)) at grain boundaries after homogenization at 585 °C for 10 min, did not change. This is the evidence that intermetallic particles at the grain boundaries result in the retardation of boundary movement.

Conclusion

1. This work shows that ex-situ techniques can be employed as an analytical technique to characterize the microstructural evolution of intermetallics that is strongly influences the mechanism of abnormal grain growth in 6063 aluminum alloys during homogenization.
2. Ex-situ SEM results with EDS applications indicated that the volume fraction and shape of β-Al_5FeSi particles were changed during homogenization and resulted in abnormal grain growth if the 6063 aluminum sample had a particle pinning parameter in the range of 0.25–1.00. Therefore, abnormal grain growth in 6063 aluminum billets relied on the remained volume fraction of intermetallics during homogenization.
3. Humphreys' model can be applied to predict grain structure during homogenization in 6063 aluminum alloy.
4. Ex-situ EBSD results indicated that abnormal grain growth in 6063

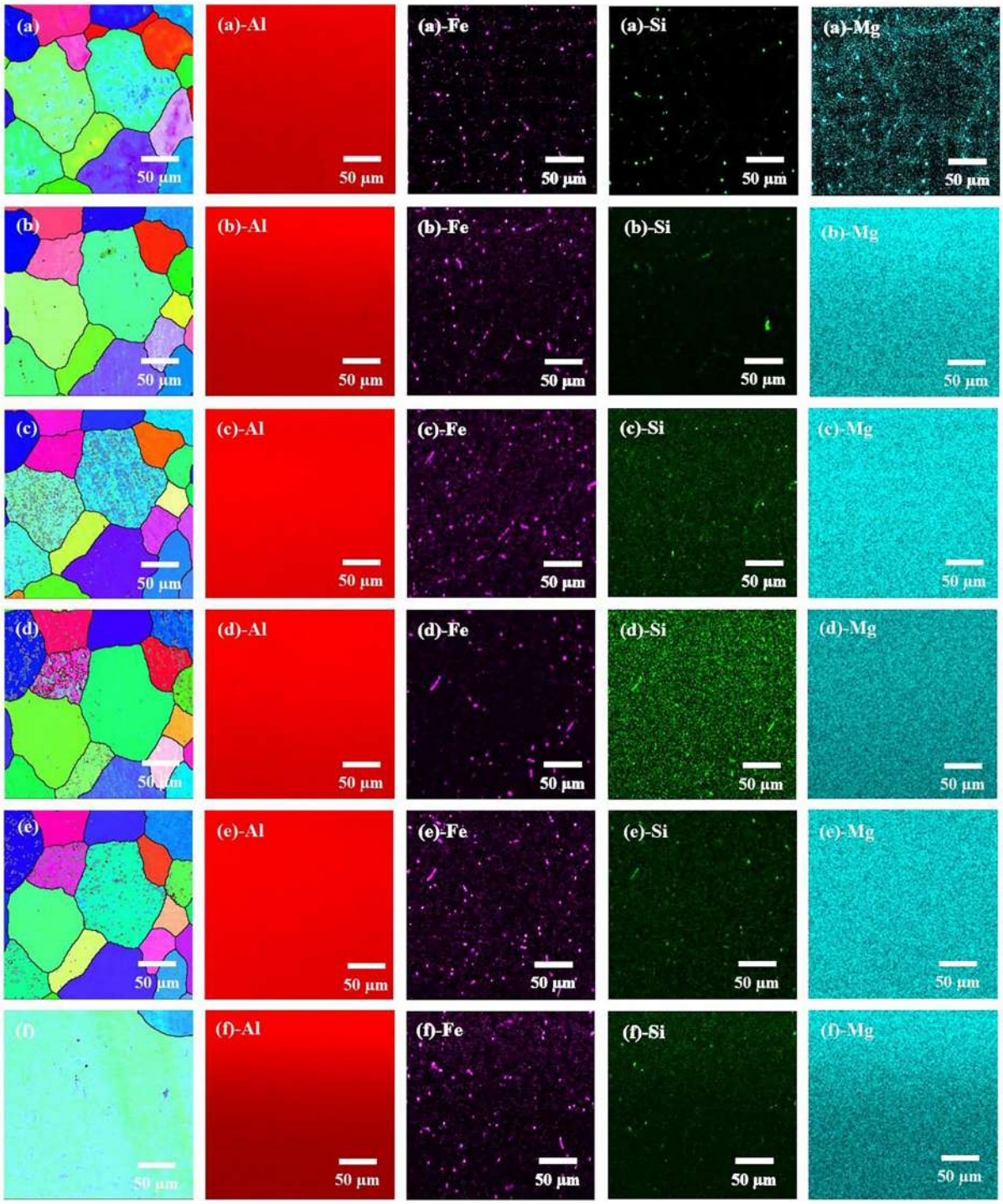

Fig. 13. EBSD micrographs for 1 sample from 6063 aluminum alloy sample I showing the aluminum phase (a) as-cast (b–f) are homogenized at 585 °C for (b) 30 min (c) 45 min (d) 60 min (e) 90 min (f) 120 min. Grain boundaries were colored in accordance with misorientation angle range: $5^\circ < \theta < 10^\circ$ = gray, $10^\circ < \theta < 15^\circ$ = brown, and $\theta > 15^\circ$ = black. (For interpretation of the references to colour in this figure legend, the reader is referred to the web version of this article.)

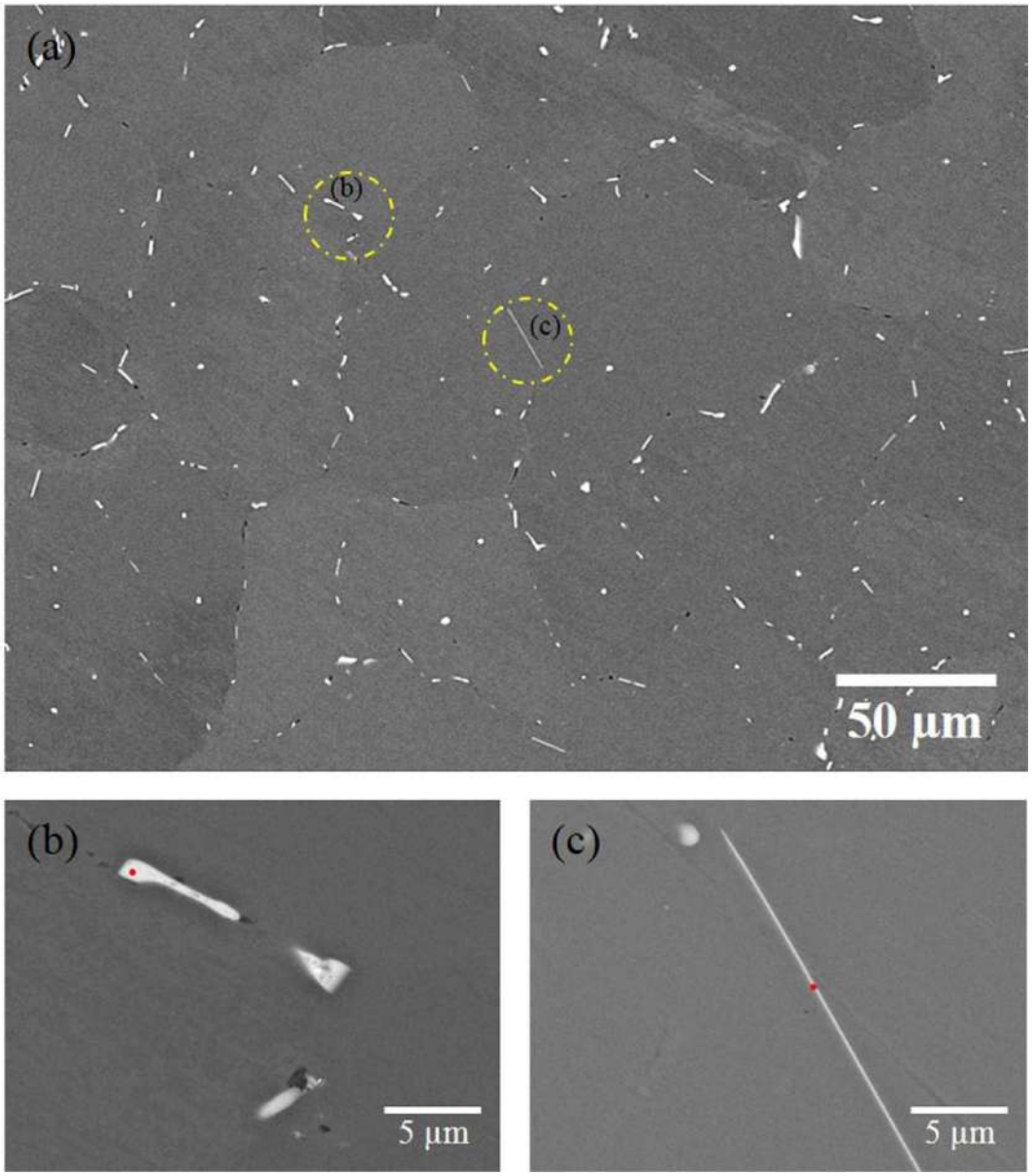

Fig. 14. BSIs of sample II after homogenization at 585 °C for 600 min.

Table 7
Corresponding elemental distribution from point (1) and (2) from Fig. 14(b) and (c).

Point	Elementary (atomic%)				Ratio	Phase
	Mg	Al	Fe	Si	Fe:Si	
(1)	–	79.93	11.04	9.03	1.22	β-Al_5FeSi
(2)	0.48	94.56	2.51	2.45	1.02	β-Al_5FeSi

aluminum billets corresponding to a high migration of high angle grain boundaries and discontinuous recrystallization.

Acknowledgments

This study is financially supported by the Thailand Research Fund (TRF) through the 'Research and Researchers for Industries Project' program (PHD57I0022) in cooperation with the CAP C.E.L. CO., LTD. The Thailand Research Fund (TRF) and the Commission on Higher Education (CHE) Grant (MRG5980253) and Chiang Mai University are also acknowledged .

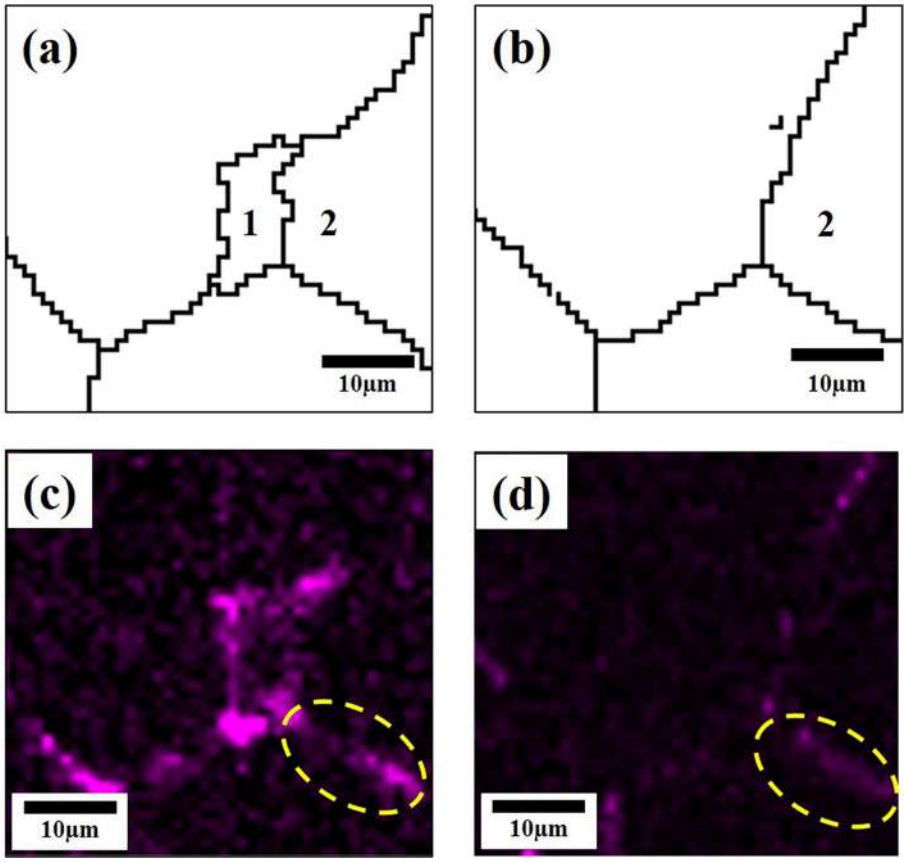

Fig. 15. (a) The high angle (misorientation angle > 15°) boundary map from EBSD of as-cast sample II and (c) its corresponding EDS map of Fe: and (b) the high angle (misorientation angle > 15°) boundary map from EBSD of sample II after homogenization at 585 °C for 10 min and (d) its corresponding EDS map of Fe.

References

[1] Humphreys FJ, Hatherly M. Recrystallization and related annealing phenomena. 2nd ed. Oxford: Elsevier; 2004.
[2] Charit I, Mishra RS. Abnormal grain growth in friction stir processed alloys. Scr Mater 2008;58:367–71.
[3] Dennis J, Bate PS, Humphreys FJ. Abnormal grain growth in Al-3.5Cu. Acta Mater 2009;57:4539–47.
[4] Chang JK, Takata K, Ichitani K, Taleff EM. Abnormal grain growth and recrystallization in Al-Mg Alloy AA5182 following hot deformation. Metall Mater Trans A 2010;41A:1949–53.
[5] Eskin DG. Physical metallurgy of direct chill casting of aluminum alloys. New York: Taylor & Francis Group; 2008.
[6] Zajac S, Hutchinson B, Johnsson A, Gullman L-O. Microstructure control and extrudability of Al-Mg-Si alloys microalloyed with manganese. Mater Sci Tech 1994;10:323–33.
[7] Polmear I. Light alloys from tradition alloys to nanocrystals. 4th ed. United Kingdom: Integra Software Pvt. Ltd; 2006.
[8] Cooksey MA, Danilova N, Rinderer B, Couper MJ. Process performance of continuous billet homogenizer. In: Whiteley PR, Grandfield JF, editors. The sixth australia asian pacific aluminum casthouse technology conference 2008. Sydney: The Minerals Metal & Materials Society; 1999. p. 309–18.
[9] Couto KBS, Claves SR, Geertruyden WHV, Misiolek WZ, Goncalves M. Effects of homogenization treatment on microstructure and hot ductility of aluminum alloy 6063. Mater Sci Tech 2005;21:263–8.
[10] Kayikci R, Kocaman E, Sirin S, Colak M. The effects of late homogenization conditions on the Mg2Si particle size in a slow preheated 6063 aluminum extrusion billet. In: 4th international congress in Advances in Applied Physics and Materials Science (APMAS 2014), American Institute of Physics, Fethiye, Turkey; 2014.
[11] Ansara I, Dinsdale AT, Rand MH. Thermochemical database for light metal alloys. Belgium: Office for Official Publications of the European Communities; 1998.
[12] Hosseinifar M, Malakhov DV. The sequence of intermetallics formation during the solidification of an Al-Mg-Si alloy containing La. Metall Mater Trans A 2011;42A:825–33.
[13] Birol Y. Formation and transformation of intermetallic particles in a strip-cast Al-0.8Fe-0.6Si alloy. Z Metallkde 1998;89:501–6.
[14] Kuijpers NCW, Kool WH, Koenis PTG, Nilsen KE, Todd I, Van der Zwaag S. Assessment of different techniques for quantification of α-Al (FeMn) Si and β-AlFeSi intermetallics in AA 6xxx alloys. Mater Charact 2003;49:409–20.
[15] Sweet L, Zhu SM, Gao SX, Taylor JA, Easton MA. The effect of iron content on the iron-containing intermetallic phases in a cast 6060 aluminum alloy. Metall Mater Trans A 2011;42A:1737–49.
[16] Gao T, Hu K, Wang L, Zhang B, Liu X. Morphological evolution and strengthening behavior of α-Al (Fe, Mn) Si in Al–6Si–2Fe–xMn alloys. Res Phys 2017;7:1051–4.
[17] Xu Y, Naguami H, Han Y, Zhang G, Zhai T. The deformation behavior and microstructure evolution of a Mn- and Cr-containing Al-Mg-Si-Cu alloy during hot compression and subsequent heat treatment. Metall Mater Trans A 2017;48:1355–65.
[18] Garcia-Bernal MA, Mishra RS, Verma R, Hernandez-Silva D. Inhibition of abnormal grain growth during hot deformation behavior of friction stir processed 5083 Al alloys. Mat Sci Eng A 2015;636:336–1330.
[19] Monteiro WA, Esposito IM, Ferrari RB, Buso SJ. Microstructure and mechanical characterization after thermomechanical treatments in 6063 aluminum alloy. Mater Sci Appl 2011;2:1529–41.
[20] Humphreys FJ. A unified theory of recovery recrystallization and grain growth, based on the stability and growth of cellular microstructures-II. The effect of second-phase particles. Acta Mater 1997;45:5031–9.
[21] Nes E, Ryum N, Hunderi O. On the Zener drag. Acta Metall 1985;33:11–22.
[22] Belov NA, Eskin DG, Aksenov AA. Multicomponent phase diagrams: applications for commercial aluminum alloys. Elsevier; 2005.
[23] Murali S, Guru Row T, Sastry D, Raman K, Murthy K. Crystal structure of beta-FeSiAl sub 5 and (beta)-BeSiFe sub 2 Al sub-phases. Scr Metall Mater 1994;31:267–72.
[24] Bayat N, Carlberg T, Cieslar M. In-situ study of phase transformations during homogenization of 6005 and 6082 Al alloys. J Alloy Compd 2017;725:504–9.
[25] Bayat N, Carlberg T, Cieslar M. In-situ study of phase transformations during homogenization of 6060 and 6063 Al alloys. J Phys Chem Solids 2019;130:165–71.
[26] Haidemenopoulos G, Kamoutsi H, Zervaki A. Simulation of the transformation of iron intermetallics during homogenization of 6xxx series extrudable aluminum alloys. J Mater Process Technol 2012;212:2255–60.
[27] Chen K, Gan W, Okamoto K, Chung K, Wagoner R. The mechanism of grain coarsening in friction-stir-welded AA5083 after heat treatment. Metall Meter Trans A 2011;42A:488–507.
[28] Jana S, Mishra RS, Baumann JA, Grant G. Effect of process parameters on abnormal grain growth during friction stir processing of a cast Al alloy. Mater Sci Eng A 2010;528:189–99.
[29] Mironov SY. About abnormal grain growth in joints obtained by friction stir welding. Met Sci Heat Treat 57 2015;40:47.
[30] Chen Y, Ding H, Li J, Cai Z, Zhao J, Yang W. Influence of multi-pass friction stir processing on the microstructure and mechanical properties of Al-5083 alloy. Mater Sci Eng A 2016;650:281–9.
[31] Park C-S, Park H-K, Shim H-S, Na T-W, Han C-H, Hwang N-M. New understanding

of the role of coincidence site lattice boundaries in abnormal grain growth of aluminum alloy. Philos Mag Lett 2015;95:220–8.
[32] Jazaeri H, Humphreys JF. The effect of initial grain size on transition from discontinuous to continuous recrystallization in a highly cold rolled Al-Fe-Mn alloy. Mater Sci Forum 2002;396–402:551–6.
[33] Jazaeri H, Humphreys F. The transition from discontinuous to continuous recrystallization in some aluminum alloys: II–annealing behavior. Acta Mater 2004;52:3251–62.
[34] Jazaeri H, Humphreys F. Quantifying recrystallization by electron backscatter. diffraction. J Microsc 2004;213:241–6.
[35] Sztwiertnia K, Bieda M, Korneva A. Continuous and discontinuous recrystallization of 6013 aluminum alloy. Mater Sci Forum 2013;753:221–4.